ISSN 1063-7729, Astronomy Reports, 2010, Vol. 54, No. 5, pp. 400–417. © Pleiades Publishing, Ltd., 2010.
Original Russian Text © G.M. Rudnitskiĭ, M.I. Pashchenko, P. Colom, 2010, published in Astronomicheskiĭ Zhurnal, 2010, Vol. 87, No. 5, pp. 444–461.

Polarization Observations of Circumstellar OH Masers

G. M. Rudnitskiĭ[1], M. I. Pashchenko[1], and P. Colom[2]

[1] *Sternberg Astronomical Institute, Universitetskiĭ pr. 13, Moscow, 119991 Russia*

[2] *LESIA, Observatoire de Paris-Meudon, 5 place Jules Janssen, Meudon, 92190 France*

Received August 12, 2009; in final form, October 19, 2009

Abstract—Results of observations of circumstellar OH masers in lines with wavelengths near 18 cm are reported. The observations were carried out on the radio telescope of the Nançay Radio Astronomy Observatory (France). In 2007–2009, 70 late-type stars were observed (including Mira and semi-regular variables). For 53 of these, emission was detected in at least one of three OH lines (1612, 1665, or 1667 MHz). Circular and linear polarization of the maser emission was measured, yielding all four Stokes parameters. Polarized emission features were detected in the OH line spectra of 41 stars. A summary of all the observations is given. The results obtained for T Lep, R LMi, and R Crt are discussed. Emission in the 1665 and 1667 MHz OH lines was detected in T Lep for the first time. Features probably due to Zeeman splitting were detected in the OH line profiles of all three stars. Estimates of the magnetic-field strengths in the maser sources were obtained (0.46–2.32 mG). Variability of the polarization characteristics of the maser emission of the stars on time intervals of several months was found.

DOI: 10.1134/S1063772910050045

1. INTRODUCTION

We study here the polarization of the maser emission in the 18-cm OH lines in the circumstellar envelopes of late-type stars, including Mira long-period variable stars and semi-regular variables [1]. The OH masers in the envelopes of late-type stars can belong to one of two classes: in class I, the most intense emission is in the main OH lines at 1665 and 1667 MHz, and in class IIb, the satellite OH line 1612 MHz has an intensity that is no less and sometimes considerably greater than the main lines. Class IIa OH sources, whose strongest emission is in the other satellite line at 1720 MHz, are not represented among late-type stars; this type of emission is characteristic of supernova remnants (W28, W44, Cas A, etc.).

The hydroxyl molecule (OH), which is widespread in cosmic conditions, has a large magnetic moment. Therefore, the observed OH line spectrum is strongly influenced by the magnetic field. This is manifest in splitting of the OH lines into strongly polarized Zeeman components. The degree of polarization of the individual components in the OH line profiles frequently reaches 100%. However, a "pure" Zeeman profile with π- and $\sigma^{\pm}$ components is almost never observed. There are often single spectral components with left- or right-circular polarization (LC and RC). The degree of polarization is high and sometimes reaches 100%. In this case, too, the polarization can have a Zeeman origin. Cook [2] and Shklovskii [3] showed that, during the propagation of the emission, one σ component can suppress the other due to instability of the maser beam.

Figure 1 shows the Zeeman pattern of the lines in the ground state of the hydroxyl molecule. Plots are given for the case when the magnetic field is parallel (left) and perpendicular (right) to the line of sight. RC and LC denote right-hand and left-hand circular polarization. The numbers above the components are their relative intensities, and the numbers under the components are the frequency shifts in units of $g_J\mu_0/h = 1.31$ MHz/G (g_J is the Landé factor, $g_J = 0.935$ for the ground rotational state of OH $^2\Pi_{3/2}$, $J = 3/2$; μ_0 is the Bohr magneton; h is Planck's constant). Table 1 lists the magnitudes of the splitting for lines connected to the ground state of the OH molecule. The Zeeman splitting of the OH lines is considered in detail in [4, 5].

Especially strongly polarized emission features are observed in the emission lines of OH masers in star-forming regions, such as W3(OH), Ori A, W49N, and W75N. The OH maser emission in late-type variable stars is not as strongly polarized, though there are interesting examples in this class of masers. Usually, circular polarization is observed; in only 10% of the objects is there also linear polarization. The polarization of features in the OH line profiles testifies to the presence of fairly strong magnetic fields with strengths of several milliGauss. If we can find features that form Zeeman pairs with opposite directions of

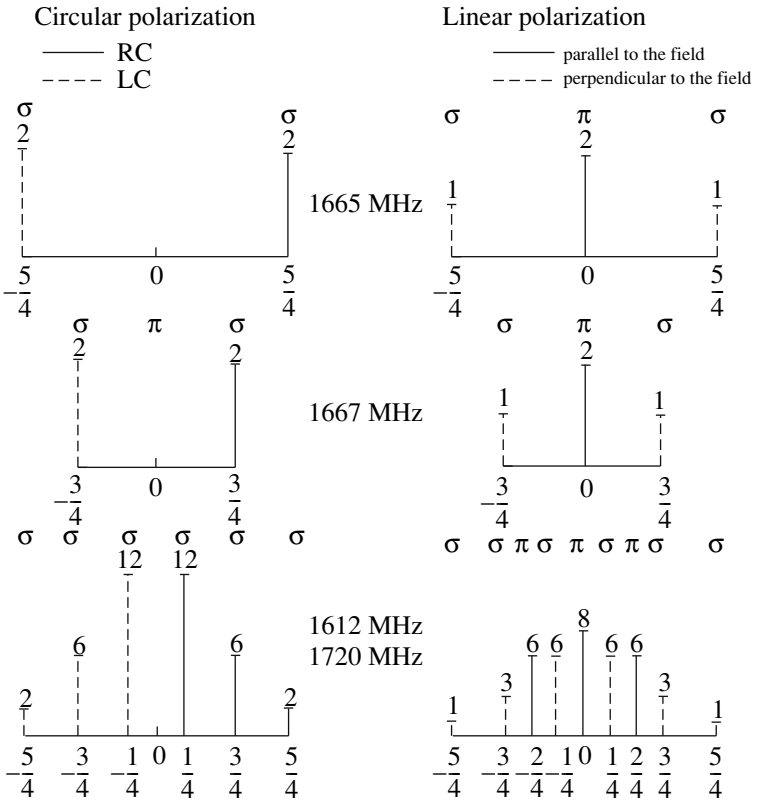

Fig. 1. Components of the Zeeman splitting for transitions between sublevels of the hyperfine structure in the Λ doubling of the ground state of the OH molecule $^2\Pi_{3/2}$ ($J = 3/2$). RC and LC denote right-hand and left-hand circular polarization.

circular polarization, they can be used to estimate the magnetic field in the source. As a rule, the profiles of the OH maser lines in long-period variable stars are simple, containing isolated emission features that are not blended with adjacent features. This simplifies the detection of probable Zeeman pairs. Multi-epoch polarization observations of the same stars can reveal possible cycles of magnetic activity.

Detailed polarimetry of seven OH masers in late-type stars was first carried out using the 305-m Arecibo radio telescope in November 1981 by Claussen and Fix [6]. They observed the Mira variable stars UX Cyg, WX Psc, IK Tau, U Ori, R LMi, R Leo, and U Her, as well as the F8 supergiant IRC+10420. All four Stokes parameters were measured. Appreciable circular and linear polarization was detected in UX Cyg, U Ori, and IRC+10420. It was concluded that linear polarization of the emission of circumstellar OH masers is less common than circular polarization. In IRC+10420, Zeeman splitting was detected for the first time in the profile of the circular polarization.

Polarization of the emission of stellar OH masers was also studied by Ukita and Le Squeren [7], who observed a sample of late-type stars on the Nançay radio telescope in November 1981 and January 1982, almost simultaneously with Claussen and Fix [6]. The measured polarization profiles were not complete, and included only a pair of linear polarizations (vertical and horizontal) or a pair of circular polarizations (LC and RC). Polarized features were detected in the OH line spectra of EY And, IRC−10529 (V1300 Aql), and IRC+70012 (V524 Cas). All three stars are classified as Mira variables in the General Catalog of Variable Stars (GCVS) [8].

Table 1. Zeeman splitting for transitions between the hyperfine structure levels in the Λ doubling of the OH ground state $^2\Pi_{3/2}$ ($J = 3/2$, σ components) according to [4]

Transition	Frequency, MHz	Zeeman splitting LC−RC	
		kHz/mG	km/s mG
$F = 1 \to 2$	1612.2310	1.308	0.236
$F = 1 \to 1$	1665.4018	3.270	0.590
$F = 2 \to 2$	1667.3590	1.964	0.354
$F = 2 \to 1$	1720.5300	1.308	0.236

Further polarization observations of circumstellar masers were conducted on the Nançay radio telescope by Szymczak and Le Squeren [9], Szymczak et al. [10, 11], and Etoka et al. [12]. In 1982–1995, Szymczak et al. [11] studied the variability of the polarization of the maser emission in the main 1667 and 1665 MHz OH lines for the three semi-regular variables (W Hya, RT Vir and R Crt).

Szymczak et al. [13, 14] obtained MERLIN polarization observations in the main 1665 and 1667 MHz OH lines for the two semi-regular variables W Hya and R Crt with an angular resolution of 0.17″. An analysis of the full polarization in all four Stokes parameters (I, Q, U, and V) enabled Szymczak et al. to determine the structure and strength of the magnetic field in the circumstellar envelope. In W Hya, the magnetic field found from the Zeeman splitting of the 1667 MHz line is ∼0.6 mG. For R Crt, differences in the polarization properties of features at negative radial velocities ($V < V_*$, "blueshifted") and at positive velocities ($V > V_*$, "redshifted") relative to the stellar velocity were detected; the former come from the near side of the expanding circumstellar envelope, and the latter from the far side. The emission of the blueshifted and redshifted features has predominantly linear and circular polarization, respectively. The explanation of this is that the emission of the redshifted features passes through inner parts of the circumstellar envelope on its way to the observer, where the electron density is enhanced. Linear polarization thus decreases due to Faraday depolarization, whereas circular polarization can be amplified. The blueshifted features are not subject to this effect. R Crt displays signs of axisymmetric expansion of its circumstellar envelope. This may suggest a role for the magnetic field in defining a preferential direction for mass loss by the star, along the magnetic-dipole axis.

In our 2007–2009 observations, we measured the full polarization of the OH maser emission (four linear polarization modes and two circular modes). This enabled us to determine simultaneously the line profiles in all four Stokes parameters. For many stars, this was the first time such observations had been done.

2. OBSERVATIONS

The observations of the late-type stars in the hydroxyl lines were conducted on the radio telescope of the Nançay Radio Astronomy Observatory (France).[1] The telescope is a Kraus-type two-mirror instrument. It is a transit telescope, enabling observation of radio sources near the meridian. The movable flat reflector with a size of 200 × 40 m directs the radio waves onto a fixed spherical mirror 300 × 35 m in size with a radius of curvature of 560 m placed at a distance of 460 m. In turn, the spherical mirror focuses the radio waves onto a feed near the ground, which is mounted on a support that can move on a rail track. The motion of the feed makes it possible to track a radio source within $\pm 30^{\mathrm{m}}/\cos\delta$ in hour angle relative to the meridian. At a declination of $\delta = 0°$, the telescope beam at 18 cm is $3.5' \times 19'$ in right ascension and declination, respectively. Observations of radio sources are possible at declinations $\delta > -39°$. The effective area of the antenna at $\lambda = 18$ cm and declination $\delta = 0°$ is 7000 m^2, and the telescope sensitivity is 1.4 K/Jy. The noise temperature of the helium-cooled amplifiers is from 35 to 60 K, depending on the observing conditions.

A recent upgrade has extended the capabilities of polarization studies [15, 16]. The radio-telescope instrumentation is able to receive emission simultaneously in four polarization modes: LC and RC, linear polarization with position angles 0° and 90° (L0° and L90°), and linear polarization with position angles 45° and −45° (L45° and L−45°). The change in the position angle of the received linear polarization is realized during the observations by rotating the feeds by 45°. Therefore, the new observations performed by us in 2007–2009 appreciably augment similar earlier polarization measurements on the Nançay radio telescope. Earlier, mainly the two circular polarization modes of the maser emission or the vertical and horizontal linear polarizations were measured [7, 11, 12]. The possibility of obtaining a complete set of polarization measurements including all four Stokes parameters has now appeared.

The spectral analysis was carried out using an 8192-channel autocorrelation spectrometer. The channels can be divided into several batteries, each of which carries out an independent signal analysis in one of two OH lines (1612 and 1667 MHz or 1665 and 1667 MHz) in one of four polarization modes. In our observations, the spectrum analyzer was divided into eight batteries with 1024 channels in each. The frequency bandwidth in each battery was 781.25 kHz, and the frequency resolution 763 Hz. This corresponds to a radial-velocity resolution of 0.137 km/s in the 1667, 1665 MHz lines and 0.142 km/s in the 1612 MHz line.

During the observations, the spectra of the two lines in LC, RC, L0°, and L90° are first recorded, after which the linear polarization feeds are rotated by 45° and the LC, RC, L45°, and L−45° spectra recorded. Thus, in a single session, we obtain eight spectra in two lines and six polarization modes (the LC and RC spectra are recorded twice and are averaged; the integration time for them is thus doubled). Combining the polarization modes, we can derive all four Stokes parameters of the OH maser emission. The Stokes

[1] http://www.obs-nancay.fr/

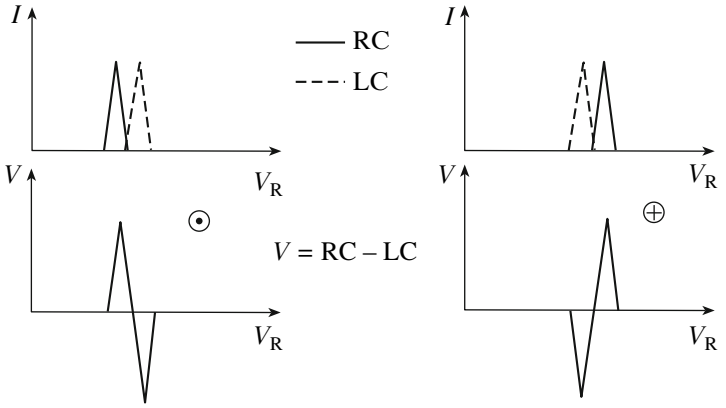

Fig. 2. Line splitting into $\sigma^{\pm}$ components in a longitudinal magnetic field. Profiles of the total intensity I with two features having 100% circular polarization of opposite directions and of Stokes V = RC − LC are schematically shown. $\odot$ denotes a field directed toward the observer and $\oplus$ a field directed away from the observer.

parameters are defined in terms of the flux densities F of the various polarizations in each frequency channel of the spectrum analyzer as follows [15]:

$$I = F(0^\circ) + F(90^\circ) = F(\mathrm{RC}) + F(\mathrm{LC}),$$
$$Q = F(0^\circ) - F(90^\circ),$$
$$U = F(45^\circ) - F(-45^\circ),$$
$$V = F(\mathrm{RC}) - F(\mathrm{LC}).$$

The degree of linear polarization is defined as

$$m_\mathrm{L} = \frac{\sqrt{Q^2 + U^2}}{I},$$

the position angle of the linear polarization as

$$\chi = \frac{180^\circ}{\pi} \arctan\left(\frac{U}{Q}\right),$$

and the degree of circular polarization as

$$m_\mathrm{C} = \frac{V}{I}.$$

As an example, Fig. 2 shows profiles of the total intensity I and Stokes parameter V for the case when the profile includes a pair of features having 100% circular polarization of opposite directions. Such a V profile is interpreted as being due to Zeeman splitting of the line, and the magnitude of the splitting characterizes the line-of-sight component of the magnetic field in the source.

3. RESULTS

The observed stars are listed in Table 2, whose columns give the names of the stars, the identification in the IRAS Point Source Catalog, the GCVS variability type [8], the radial velocities of the stars relative to the Local Standard of Rest (V^*_LSR), the studied range of V_LSR, the Julian dates of the observations, and the peak flux densities F_max and radial velocities V_LSR of emission features observed in the 1612, 1665, and 1667 MHz OH lines. Polarized features are marked by a superscript "p." Flux densities with "$<$" in the last three columns are upper limits (at the 3σ level) for the flux density in the corresponding line in the entire observed range of radial velocities. With integration times from 10 to 40 min, the upper limits were typically from 0.1 to 0.2 Jy (1 Jy = 10^{-26} W m^{-2} Hz^{-1}).

We observed 70 stars from October 2007 to June 2009. Emission in at least one of the three OH lines—1612, 1665 or 1667 MHz—was detected in 53 of these. Appreciable polarization (nonzero Stokes parameters Q, U, or V) was present in 41 stars.

Figures 3–5 show the profiles of the Stokes parameters I, Q, U and V for three stars displaying the characteristic polarization of the maser emission in the OH lines. We comment on these stars in the following section.

4. DISCUSSION

4.1. T Lep

T Lep is a long-period Mira variable with a period of $P = 368.13^\mathrm{d}$ [8]. The analysis of the light curve of the data of the American (AAVSO[2]) and French (AFOEV[3]) associations of variable star observers demonstrates that the period has not changed. The estimated distance is 377 pc [17]. The star was poorly studied in the hydroxyl lines. te Lintel Hekkert et al. [18] observed T Lep in the 1612 MHz line in April–May 1986 during a survey of point-like infrared

[2] http://www.aavso.org/
[3] http://cdsarc.u-strasbg.fr/ftp/cats/afoev/lep/t

Table 2. Stars observed in the OH lines on the Nançay Radio Telescope

Star	IRAS	Variability type	V^*_{LSR}, km/s	V_{LSR} range, km/s	Date, JD−2454000	F_{max}, Jy/V_{LSR}, km/s		
						1612 MHz	1665 MHz	1667 MHz
1	2	3	4	5	6	7	8	9
Y Cas	00007+5524	M	−26.2	−51 . . . +19	488	<0.2		3/−22^p
								5/−12^p
TY Cas	00340+6251	M	−59	−94 . . . −24	425	<0.2		<0.2
				−94 . . . −24	988	<0.2	<0.2	<0.2
WX Psc	01037+1219	M	+10	−14 . . . +58	425	33/−9^p		5/−10^p
						32/+27^p		6/+26^p
V669 Cas	01304+6211	M	−55	−90 . . . −19	425	208/−66^p		2/−65
						38/−43^p		35/−44^p
				−90 . . . −19	988	318/−66^p	0.6/−66	1.5/−66
						63/−44^p		40/−44^p
V370 And	01556+4511	SRb	−7	−42 . . . +28	425	<0.2		<0.2
				−42 . . . +28	445	<0.2		<0.2
S Per	02192+5821	SRc	−45.2	−80 . . . −10	464	3/−51^p		8/−52^p
						1/−26^p		1/−27
				−75 . . . −5	746	2.5/−51	13/−52^p	8/−52^p
						2.7/−23	1.0/−26	1.0/−21
R Tri	02339+3402	M	+59	+24 . . . +94	464	<0.2		<0.2
RU Ari	02420+1206	M	+20	−38 . . . +32	445	1/+16		0.25/+16
						3.4/+24		1/+24
				−15 . . . +55	752	1.5/+16		0.5/+16
						4/+24		2/+25
U Ari	03082+1436	M	−57	−92 . . . −22	426	<0.2		<0.2
				−92 . . . −22	470	<0.2		<0.2
IK Tau	03507+1115	M	+33.5	−10 . . . +60	426	15/+17^p		12/+17^p
						12/+51^p		13/+51^p
W Eri	04094−2515	M	−0.3	−35 . . . +35	471	<0.2		0.3/−4
								0.9/+4
R Tau	04255+1003	M	+15.5	−19 . . . +51	426	<0.2		0.2/+10
								0.4/+18
TX Cam	04566+5606	M	+13	−22 . . . +48	426	<0.2		<0.2
T Lep	05027−2158	M	−30	−63 . . . +7	561	<0.2		0.4/−31
				−65 . . . +5	757		0.5/−30^p	0.2/−31
				−65 . . . +5	836	<0.2	0.9/−30^p	0.9/−31^p
				−65 . . . +5	946		0.4/−36^p	
							0.6/−30^p	0.3/−31^p
NV Aur	05073+5248	M	+4	−31 . . . +39	453	10/−14		1.8/−13
						24/+20^p		1.6/+19
BW Cam	05151+6312	M	+50	+15 . . . +85	571	7/+37		0.4/+66
						3/+67		

Table 2. (Contd.)

Star	IRAS	Variability type	V^*_{LSR}, km/s	V_{LSR} range, km/s	Date, JD−2454000	F_{max}, Jy/V_{LSR}, km/s		
						1612 MHz	1665 MHz	1667 MHz
1	2	3	4	5	6	7	8	9
U Aur	05388+3200	M	+8.5	−26 . . . +44	946	<0.2	1.5/+3^p	1.0/+3^p
							0.5/+11	1.0/+11
U Ori	05528+2010	M	−35.9	−71 . . . −1	426	<0.2		0.5/−41^p
								1/−35^p
AP Lyn	06300+6058	M	−22	−53 . . . +17	550	1.1/−35		0.2/−25
						0.25/−10		0.2/−11
U Lyn	06363+5954	M	−9	−44 . . . +26	561	<0.2		0.5/−17
GX Mon	06500+0829	M	−10	−51 . . . +19	571	0.9/−28^p		1.2/−28
						3.4/+7		1.6/+7
				−45 . . . +25	820		<0.2	5.9/−28^p
								4.2/+7
				−45 . . . +25	836	5.3/−28	0.2/+10	5.3/−28^p
						9.2/+7^p		4.2/+7
VY CMa	07209−2540	L	+21.47	−13 . . . +57	403	610/−11^p		112/−9^p
						1283/−4^p		365/−1^p
						426/+45^p		19/+47^p
Z Pup	07304−2032	M	−0.35	−35 . . . +35	426	0.3/−3		2.7/−2.5^p
								0.7/+5
								0.7/+12
HU Pup	07536−2830	SRa	+44	+9 . . . +79	403	2.3/+42^p		1.2/+34^p
								0.36/+39
								0.37/+42
								0.3/+63
				+9 . . . +79	562	6.6/+42^p		1.4/+34^p
								1/+39^p
								1/+41^p
								0.25/+63
				+9 . . . +79	955		0.8/+34^p	0.6/+35^p
							0.3/+37^p	1.0/+39^p
						8.6/+42^p	4.2/+40^p	0.6/+41^p
							0.5/+42^p	0.1/+63
U Pup	07585−1242	M	−13	−48 . . . +22	403	<0.2		0.5/−20
R Cnc	08138+1152	M	+13	−22 . . . +48	426	<0.2		6.6/+11^p
								0.5/+14
								0.5/+15
				−22 . . . +48	591	<0.2		2/+11.5^p
								0.3/+15
				−4 . . . +31	985	<0.2	1.1/+14^p	0.3/+15

Table 2. (Contd.)

Star	IRAS	Variability type	V^*_{LSR}, km/s	V_{LSR} range, km/s	Date, JD−2454000	F_{max}, Jy/V_{LSR}, km/s		
						1612 MHz	1665 MHz	1667 MHz
1	2	3	4	5	6	7	8	9
SV Pup	08149−1339	M	+30	−5 . . . +65	453	<0.2		<0.2
S Hya	08509+0315	M	+70	+35 . . . +105	426	<0.2		<0.2
IRC−20176	08534−1901		+4	−31 . . . +39	602	<0.2		<0.2
X Hya	09331−1428	M	+27	−8 . . . +62	426	<0.2		<0.2
R LMi	09425+3444	M	−0.8	−36 . . . +34	471	<0.1		2.6/−3^p
								2.0/+5^p
				−36 . . . +34	946		5.6/−4^p	2.5/−4^p
							1.1/+5	1.4/+5^p
IW Hya	09429−2148	M	+40	+11 . . . +81	550	8/+27^p		0.9/+27
						6/+51^p		
R Leo	09448+1139	M	+1	−34 . . . +36	426	<0.2		0.2/+5
				−34 . . . +36	596	<0.2		0.45/+5
V Ant	10189−3432	M	−18	−53 . . . +17	426	0.5/−21		1.2/−22
						2.2/−14		0.7/−19
								2.7/−14^p
								1.3/−12
VX UMa	10521+7208	M	−50.7	−86 . . . −16	549	1.3/−55		1.9/−54
						2.3/−45^p		1.0/−45
R Crt	10580−1803	SRb	+10.2	−18 . . . +52	426	<0.2		2.7/+3^p
								0.5/+13^p
								0.3/+17^p
								0.5/+20^p
				−18 . . . +52	469	<0.2		1.9/+3^p
								0.6/+13^p
								0.4/+17^p
								0.3/+20^p
S Crt	11501−0719	SRb	+38.5	+4 . . . +74	426	<0.2		<0.2
				+4 . . . +74	550	<0.2		<0.2
R Com	12016+1903	M	−4	−39 . . . +31	471	<0.2		0.2/−8
T Vir	12120−0545	M	+7	−28 . . . +42	426	0.5/+5		<0.2
						0.4/+12		
U CVn	12449+3838	M	−23	−58 . . . +12	426	0.5/−19		0.3/−27
								0.7/−19
RT Vir	13001+0527	SRb	+14	−21 . . . +49	470	0.2/+24		0.3/+14^p
								1.3/+24^p
				−21 . . . +49	549	0.25/+23		0.5/+24
W Hya	13462−2807	SRa	+40	+5 . . . +75	425	<0.2		0.9/+34^p
								16/+36^p

Table 2. (Contd.)

Star	IRAS	Variability type	V^*_{LSR}, km/s	V_{LSR} range, km/s	Date, JD−2454000	F_{max}, Jy/V_{LSR}, km/s		
						1612 MHz	1665 MHz	1667 MHz
1	2	3	4	5	6	7	8	9
RU Hya	14086−2839	M	−3.6	−38 . . . +32	471	1.4/−5		2.6/−7^p
						0.6/+2		1.3/+1
				−38 . . . +32	550	1.0/−5		1.2/−7^p
						0.4/+1		0.4/+1^p
				−38 . . . +32	957	0.5/−5	0.4/−6	0.8/−7
						0.5/+2	0.6/0	0.4/+1
RX Boo	14219+2555	SRb	+1.05	−34 . . . +36	471	<0.2		<0.2
RS Vir	14247+0454	M	−14	−49 . . . +21	425	2.3/−18		0.5/−17
						2.2/−16		0.5/−16
						6.6/−10^p		0.6/−14
								2.0/−10^p
Y Lib	15090−0549	M	+11.4	−23 . . . +47	425	<0.1		0.21/+11
S CrB	15193+3132	M	+1.16	−35 . . . +37	470	6.8/−2		2.6/−0
						4.7/+4		11/+4^p
WX Ser	15255+1944	M	+6	−34 . . . +36	598	4.7/−1		
						5.0/+14		0.7/+13
FS Lib	15576−1212	M	−12	−47 . . . +23	425	1.0/−12		0.3/−4^p
						1.7/+6		
				−47 . . . +23	958	0.7/−12		0.4/−11
						1.1/+6		0.2/−4
U Her	16235+1900	M	−15	−50 . . . +20	442	0.8/−20		7/−20^p
						0.5/−9		3.5/−11^p
				−50 . . . +20	550	0.5/−20		4.6/−20^p
						0.4/−9		3.5/−11^p
				−50 . . . +20	697		8/−20^p	6/−20^p
							3.3/−10^p	4.6/−9^p
V697 Her	16260+3454	M	+55	+11 . . . +81	471	4.7/+42		
						3.2/+68		0.6/+68
				+20 . . . +90	590	3.8/+42		<0.2
						2.6/+68		
VX Sgr	18050−2213	SRc	+5	−39 . . . +31	696	104/−14^p		33/−4^p
						106/+25^p		13/+19^p
IRC−10414	18204−1344		+40	+10 . . . +80	940	1.9/+36^p	4.1/+27^p	7.0/+29^p
						1.1/+48^p	2.2/+30^p	1.9/+54^p
						4.2/+56^p	2.3/+34^p	2.4/+58^p
							1.3/+46^p	
							1.9/+53^p	

Table 2. (Contd.)

Star	IRAS	Variability type	V^*_{LSR}, km/s	V_{LSR} range, km/s	Date, JD−2454000	F_{max}, Jy/V_{LSR}, km/s		
						1612 MHz	1665 MHz	1667 MHz
1	2	3	4	5	6	7	8	9
R Aql	19039+0809	M	+47	+12 . . . +82	525	8/+41		$4.6/+42^p$
						$63/+54^p$		$2.7/+44^p$
V3880 Sgr	19059−2219	M	+22	−21 . . . +49	726	$16/+9^p$		0.2/+8
						$6/+35^p$		0.5/+36
RT Aql	19356+1136	M	−28	−63 . . . +7	553	<0.2		1.1/−34
								0.8/−25
				−63 . . . +7	814		$1.9/-34^p$	1.0/−34
							$0.6/-25^p$	1.2/−25
V391 Cyg	19394+4840	M	−22.5	−57 . . . +13	403	0.8/−27		<0.2
						1.2/−25		
						$6/-21^p$		
						0.7/−3		
RR Aql	19550−0201	M	+29.1	−6 . . . +64	404	2.0/+21		1.1/+22
						$12/+23^p$		$7/+24^p$
						$7/+24^p$		3.1/+26
						$13/+33^p$		$2.7/+29^p$
						$6/+34^p$		1.6/+32
SY Aql	20047+1248	M	−48.5	−83 . . . −13	403	$5.4/-50^p$		1.7/−52
						2.4/−44		$1.8/-44^p$
KY Cyg	20241+3811	Lc	−3	−38 . . . +32	806	<0.2		<0.2
DR Cyg	20417+3759	M	+12.9	−22 . . . +48	403	<0.2		<0.2
NML Cyg		M	−19.6	−54 . . . −16	404	$985/-25.4^p$		1.1/−28.2
						$1921/-24.1^p$		$5.2/-14.0^p$
						$706/-20.9^p$		1.8/−6.2
						$733/-19.5^p$		2.5/−4.2
						$246/-17.3^p$		3.9/+0.7
						$90/-13.6^p$		3.8/+10.6
						$106/+8.2^p$		5.3/+13.9
						$108/+10.2^p$		4.5/+22.4
						$253/+20.4^p$		$7.0/+24.8^p$
						$328/+21.8^p$		
UX Cyg	20529+3013	M	−2.7	−38 . . . +32	525	0.9/−12		0.6/−12
						0.2/−6		$0.3/-1^p$
						0.3/−3		0.3/+6
						0.4/+12		0.2/+14

Table 2. (Contd.)

Star	IRAS	Variability type	V^*_{LSR}, км/с	V_{LSR} range, km/s	Date, JD−2454000	F_{max}, Jy/V_{LSR}, km/s		
						1612 MHz	1665 MHz	1667 MHz
1	2	3	4	5	6	7	8	9
UU Peg	21286+1055	M	+24	−11 . . . +59	806	0.2/+19		$6.8/+19^p$
								$13/+21^p$
								$2.6/+30^p$
				−11 . . . +59	814		$2.8/+19^p$	$6.5/+19^p$
							$7.8/+21^p$	$12/+21^p$
							$1.3/+28^p$	$2.7/+30^p$
							$2.2/+30^p$	
				−11 . . . +59	935	<0.2	$2.2/+19^p$	$5.5/+19^p$
							$6.2/+21^p$	$12/+21^p$
							$1.2/+28^p$	
							$1.7/+30^p$	$2.1/+30^p$
				−11 . . . +59	958	<0.2	$1.8/+19^p$	$4.8/+19^p$
							$5.5/+21^p$	$9.0/+21^p$
							$0.8/+28^p$	
							$1.5/+30^p$	$1.8/+30^p$
TW Peg	22017+2806	SRb	−7.8	−43 . . . +27	403	<0.2		<0.2
IRC+60370	22480+6002	M?	−50.3	−85 . . . −15	419	<0.2		<0.2
				−85 . . . −15	525	<0.2		<0.2
V627 Cas	22556+5833	SR:	−52	−81 . . . −11	403		0.5/−59	0.4/−56
							0.5/−54	$0.5/-53^p$
							$1.1/-51^p$	0.4/−49
				−81 . . . −11	727		0.2/−59	$1.4/-52^p$
							$0.9/-53^p$	$0.4/-51^p$
							$0.7/-51^p$	
							$0.6/-49^p$	
							$0.3/-46^p$	
				−81 . . . −11	814	0.9/−59		$0.7/-52^p$
R Peg	23041+1016	M	+27.85	−7 . . . +63	403	<0.2		0.4/+20
								0.2/+27
				−7 . . . +63	420	<0.2		0.3/+20
								0.2/+30
PZ Cas	23416+6130	SRc	−39.5	−74 . . . −4	401	$9/-65^p$		<0.2
						$11/-12^p$		
R Cas	23558+5106	M	+21.4	−7 . . . +63	402		0.5/+20	1.2/+21
							$3.0/+31^p$	$1.3/+31^p$
				−7 . . . +63	569	<0.2		0.7/+21
								1.2/+32
				−7 . . . +63	943			0.4/+21
							$1.0/+31^p$	0.8/+32

Note: A superscript "p" denotes polarized features.

sources from the IRAS catalog on the 64-m Parkes antenna (Australia). They appear to have detected faint emission. The line profile was typical of Class IIb OH masers, and consisted of two emission features at radial velocities $V_{\rm LSR} = -15.9$ and -0.2 km/s with peak flux densities of 0.73 and 0.36 Jy, respectively. Searches for emission of T Lep in the main OH lines carried out since January 1989 on the Nançay Radio Telescope [19] have yielded no positive results (with upper limits at the 3σ level being $\sim$0.06 Jy). T Lep is also a source of SiO [20] and H_2O [21] maser emission.

We observed T Lep in the OH lines four times: on April 4, 2008 (light-curve phase $\varphi = 0.30$), October 17, 2008 ($\varphi = 0.83$), January 4, 2009 ($\varphi = 0.04$), and April 24, 2009 ($\varphi = 0.34$). No appreciable 1612 MHz emission was detected on April 4, 2008 and January 4, 2009 (there may be faint emission at $V_{\rm LSR} = -6.9$ km/s with a peak flux density of $F_{\rm max} = 0.3$ Jy in the I 1612 MHz spectrum of April 4, 2008).

We detected for the first time emission of T Lep in the main OH lines at 1665 and 1667 MHz (Fig. 3, Table 2). In all measured profiles of the main OH lines, the emission is represented by a single feature. In the 1667 MHz spectra of April 4, 2008 and October 17, 2008, an unpolarized feature is present at $V_{\rm LSR} \approx -31$ km/s (close to the stellar velocity, $V^*_{\rm LSR} = -30$ km/s), with flux densities of $F_{\rm max} = 0.5$ and 0.2 Jy, respectively. The 1665 MHz feature observed on October 17, 2008 has $F_{\rm max} = 0.5$ Jy at $V_{\rm LSR} \approx -30$ km/s and RC with the degree of circular polarization $m_{\rm C} \approx 0.5$.

In the spectra for January 4, 2009, the 1665 and 1667 MHz emission features have approximately equal intensities ($F_{\rm max} = 0.9$ Jy). The 1667 MHz feature has LC polarization with $m_{\rm C} \approx 0.44$. The profile of the Stokes parameter $V = F({\rm RC}) - F({\rm LC})$ of the 1665 MHz feature has structure characteristic of Zeeman splitting[4] (Fig. 2). The maxima of the emission in RC and LC are at $V_{\rm LSR} = -30.20$ and -30.47 km/s, respectively. This splitting of the 1665 MHz line may be due to the magnetic field in the masing region, implying a field that is directed along the line of sight away from the observer and has a strength of $\sim$0.46 mG. Its 1667 MHz counterpart at $V_{\rm LSR} = -30.55$ km/s with $F_{\rm max} = 0.9$ Jy is circularly polarized. The V profile contains a single negative spike, with $m_{\rm C} \approx 0.5$.

Finally, in the April 24, 2009 session, the 1665 MHz profile contains two narrow emission features at $V_{\rm LSR} \approx -30.1$ and -35.6 km/s with $F_{\rm max} = 0.6$ and 0.45 Jy, respectively. Both features are circularly polarized (positive spikes in the V profile) with $m_{\rm C} \sim 0.5$. In the 1667 MHz line, there is a single unpolarized feature at $V_{\rm LSR} = -30.96$ km/s with $F_{\rm max} = 0.34$ Jy.

Thus, the polarization characteristics of the OH emission of T Lep changed during our observation interval. This could be related to the brightness cycle of the star. According to the AAVSO data, T Lep passed its maximum at JD $\approx$ 2 454 820 (December 19, 2008). Our observation of January 4, 2009, took place soon after the maximum of its visual brightness ($\varphi = 0.04$), when an increase in $F_{\rm max}$ and degree of polarization of the emission was recorded.

Note that the data on the 1612 MHz line of [18] are not consistent in terms of $V_{\rm LSR}$ with our results and with the observational data on T Lep in lines of SiO [20, 22, 23] and H_2O [21]. In all these papers, the maser emission features are concentrated at velocities from $V_{\rm LSR} \sim -27$ to -31 km/s, near the radial velocity $V^*_{\rm LSR}$ of T Lep. In late-type stars, the velocities of two emission features in the 1612 MHz OH profiles corresponding to the maximum expansion velocity of the circumstellar envelope relative to the radial velocity $V^*_{\rm LSR}$ of the central star restrict the $V_{\rm LSR}$ range for the emission in the main OH lines and in the lines of other molecules. However, the velocities of the two 1612 MHz features (-15.9 and -0.2 km/s) claimed for T Lep by Te Lintel Hekkert et al. [18] are far from $V^*_{\rm LSR}$, and do not encompass the velocity interval of the emission in other lines. However, Te Lintel Hekkert et al. [18] call the detection of the 1612 MHz emission in T Lep only "tentative." Therefore, we consider T Lep to be a newly discovered Class I OH maser.

4.2. R LMi

R LMi is a long-period Mira variable with a period of $P = 372.19^{\rm d}$ [8]. The AAVSO and AFOEV data for R LMi in the interval JD = 2 450 000–2 455 000 confirm the GCVS period. The distance to R LMi is 260 pc [24]. Emission in the 1667 MHz OH line was detected in July 1971 by Wilson and Riegel [25]. Independently, the 1665/1667 MHz OH maser in R LMi was discovered in May 1972 on the Nançay Radio Telescope by Fillit et al. [26].

We observed R LMi twice (Fig. 4): on January 5, 2008, in the 1612 and 1667 MHz lines (at phase $\varphi = 0.08$) and on April 24, 2009 in the 1665 and 1667 MHz lines ($\varphi = 0.34$). The 1667 MHz line (and in the latter epoch the 1665 MHz line) has a profile characteristic of late-type stars: two peaks generated in the expanding circumstellar envelope and located

[4] A Zeeman-like pattern is also outlined in the 1665 MHz V profile for October 17, 2008, but, in contrast to the January 4, 2009 profile, the signal-to-noise ratio is lower and the negative spike in V is pronounced more weakly.

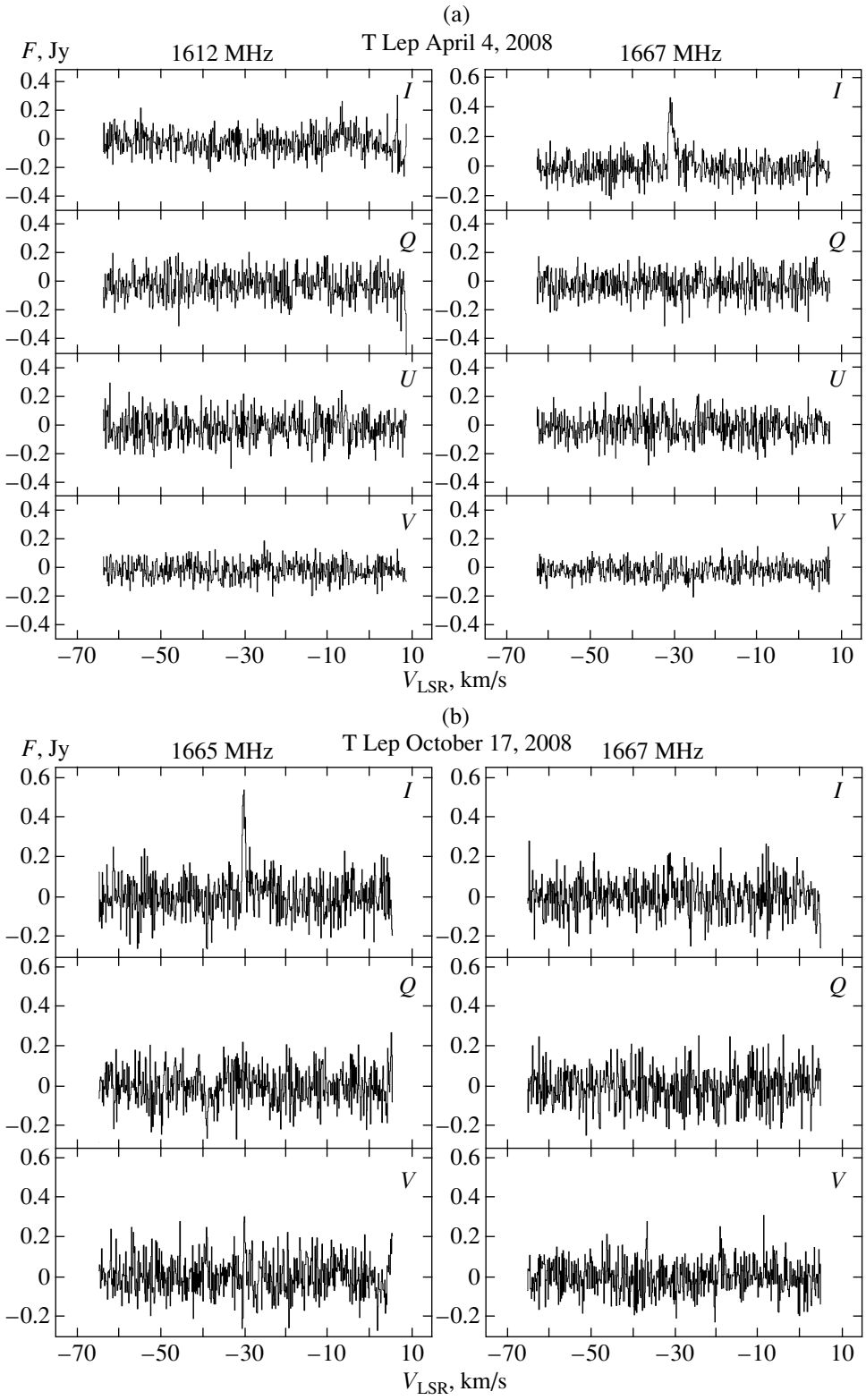

Fig. 3. Profiles of Stokes parameters of the OH lines of T Lep.

on either side of the stellar radial velocity V^*_{LSR} (for R LMi, $V^*_{LSR} = -0.8$ km/s).

In our first observing session on January 5, 2008, no emission was detected in the 1612 MHz line

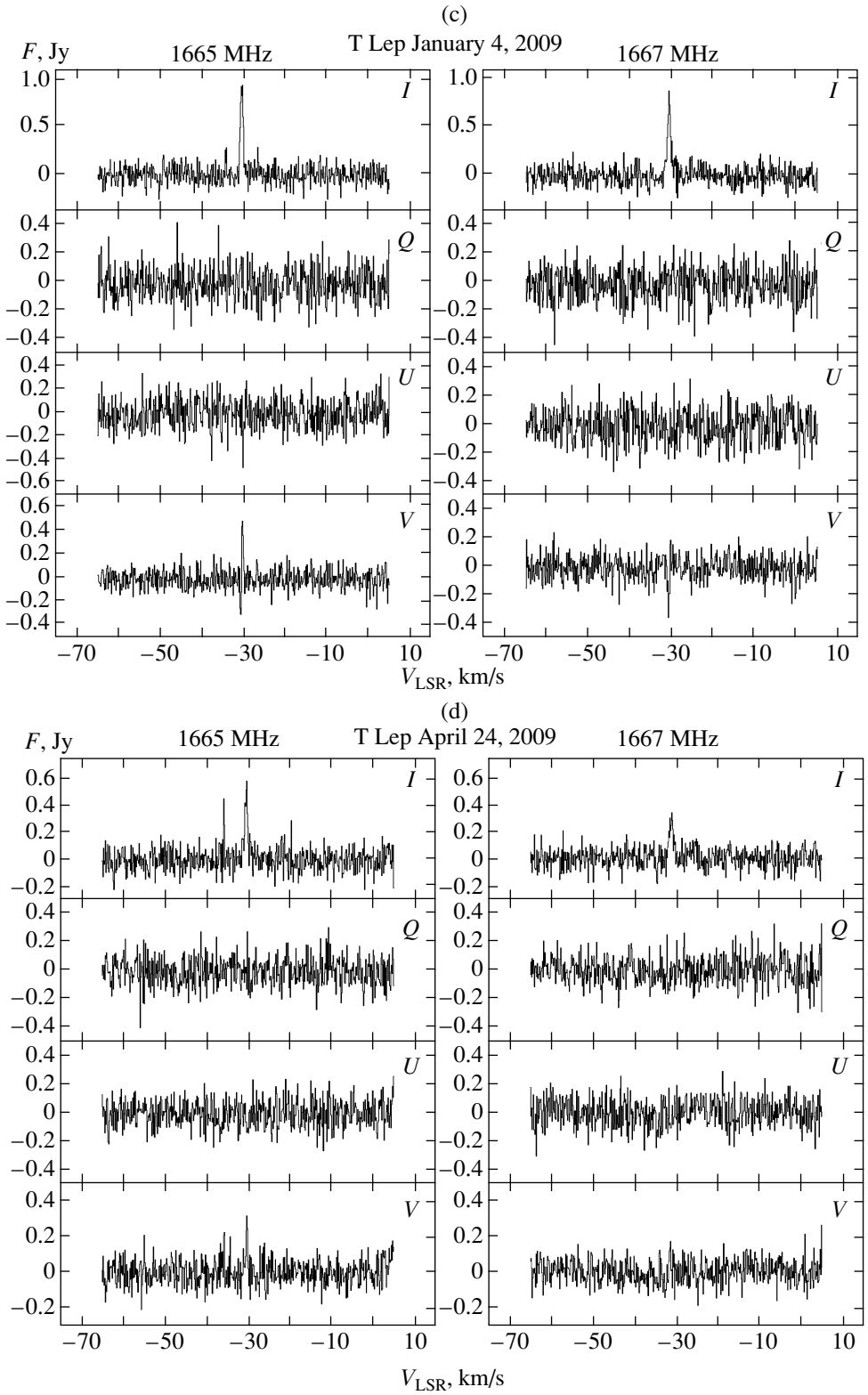

Fig. 3. (Contd.)

($F_{max} < 0.2$ Jy): the OH maser in R LMi also belongs to Class I. The 1667 MHz line profiles consist of two peaks at $V_{LSR} = -3$ and +5 km/s with $F_{max} = 2.6$ and 2.0 Jy. In the V profile, the redshifted

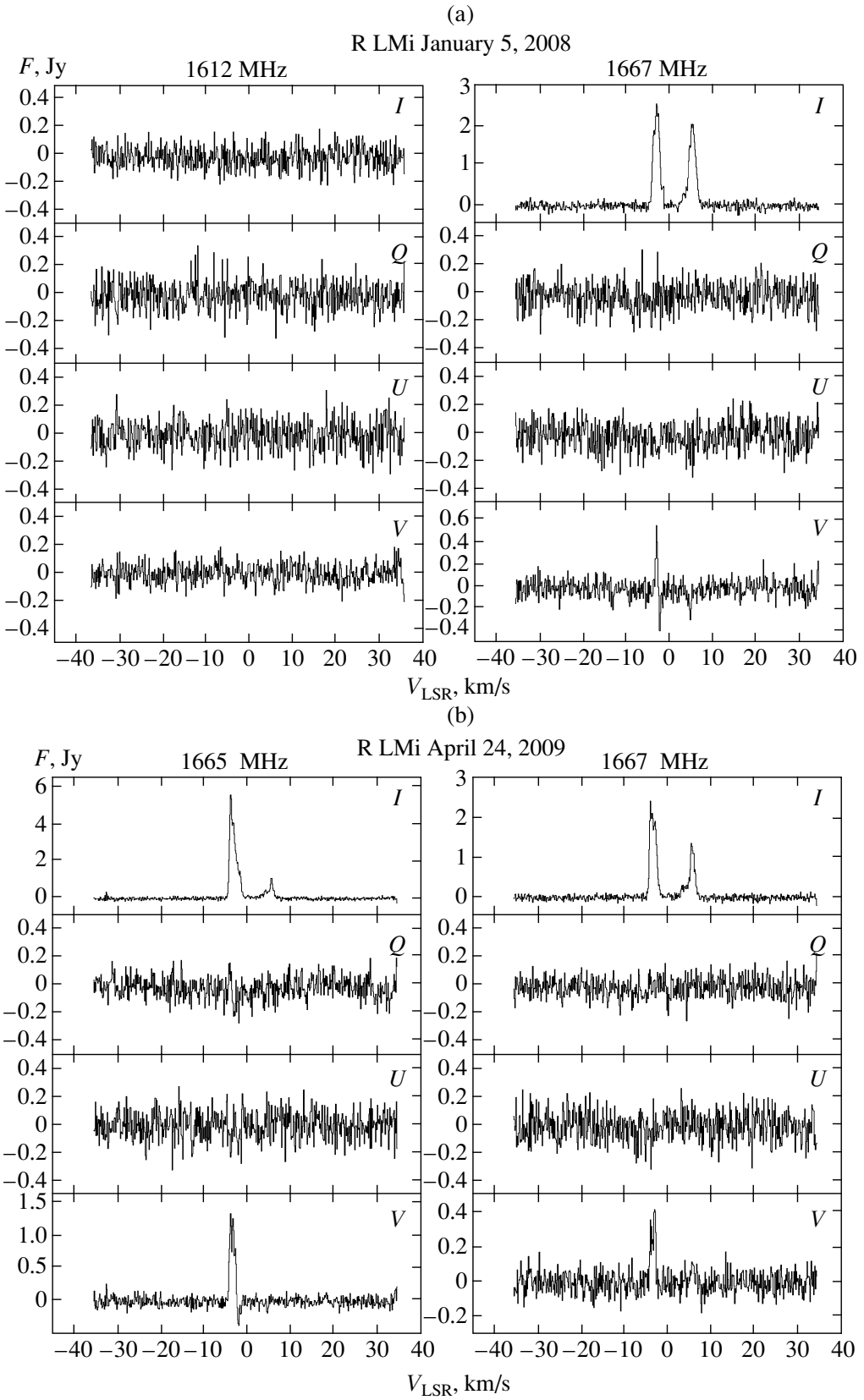

Fig. 4. Profiles of Stokes parameters of the OH lines of R LMi.

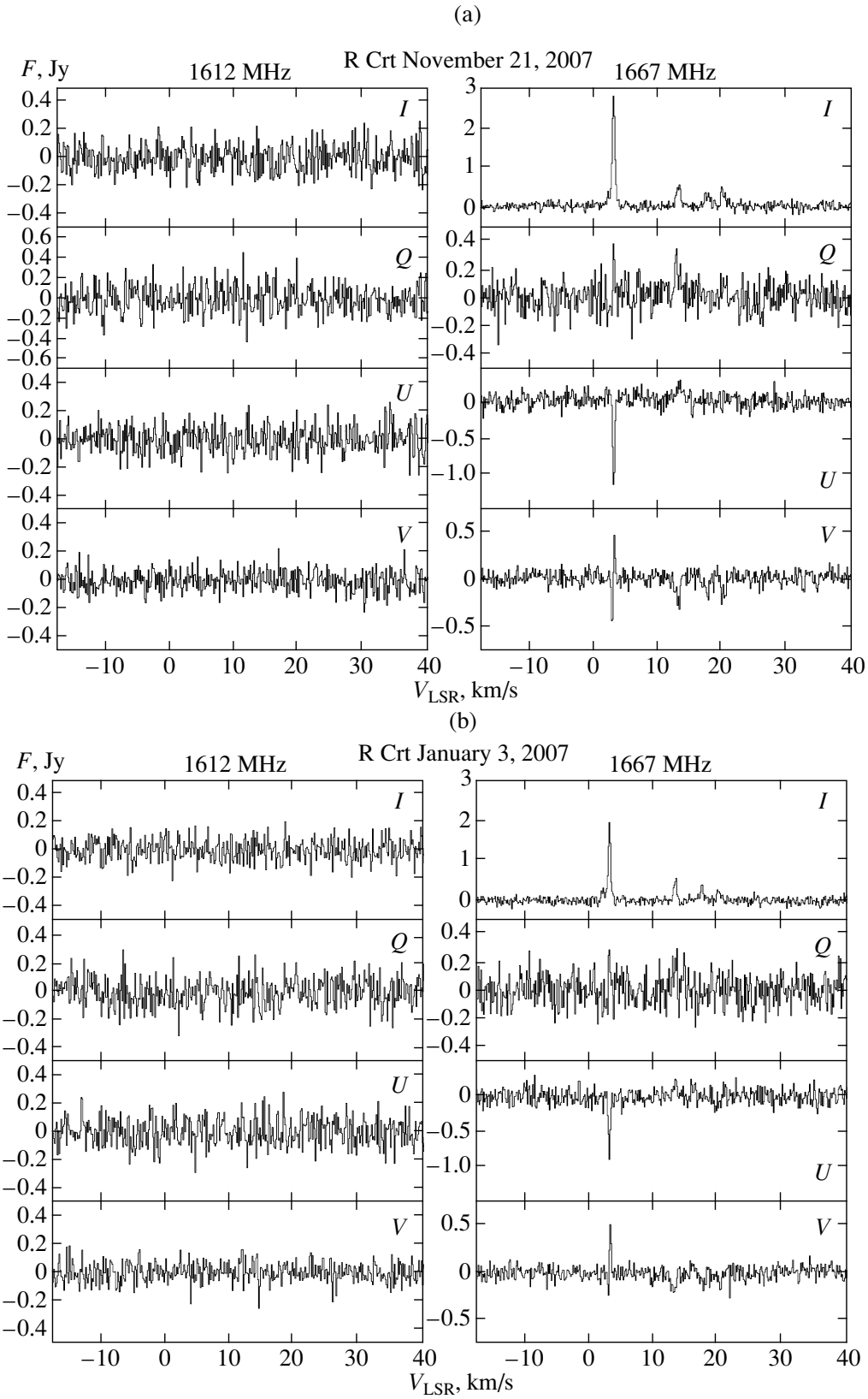

Fig. 5. Profiles of Stokes parameters of the OH lines of R Crt.

wing of the feature at −3 km/s has a counterpart such as is shown in Fig. 2 at the left. The maxima of the emission in RC and LC are $V_{\rm LSR} = -3.13$ and −2.31 km/s, respectively. This splitting could be due to a magnetic field in the masing region directed along the line of sight toward the observer with a strength of ∼2.32 mG. The feature in the I profile at +5 km/s also has a counterpart in the V profile, with $m_{\rm C} \sim 0.20$.

In the April 24, 2009 session (the descending branch of the light curve) the amplitude of the 1667 MHz features at −3 and +5 km/s decreased to 2.4 and 1.4 Jy, respectively. The V profile simultaneously changed: the features at −3 km/s and +3 km/s were completely positive (without a Zeeman pattern). This suggests a modification in the structure of the magnetic field in the masing region. In the 1665 MHz line, there are also two maxima at $V_{\rm LSR} = -4.1$ km/s ($F_{\rm max} = 5.6$ Jy) and $V_{\rm LSR} = +5.3$ km/s ($F_{\rm max} = 1.1$ Jy). The latter feature is unpolarized, while the former is circularly polarized, displaying a positive counterpart in the V profile with $m_{\rm C} \approx 0.24$. There is a small negative outburst in the red wing of the feature in the V profile. This may represent part of a Zeeman pattern; however, the positive part of the pattern is blended with the stronger main feature. Therefore, it is difficult to estimate the magnitude of splitting and the magnetic field from the 1665 MHz V profile.

4.3. R Crt

R Crt is an SRb-type semi-regular variable with an intermediate-term variability cycle of $160^{\rm d}$ [8]. The estimated distance to the star is 186 pc [27]. Its brightness variations are irregular. According to the AAVSO and AFOEV data (which have long gaps), the visual brightness of the star changed chaotically in the interval JD = 2 447 000–2 448 000 within 8.5^m–10^m. Further, in JD = 2 449 000–2 451 000, the brightness was at a level of 9.20^m–9.25^m. About JD = 2 452 000, there was a short rise in the brightness to 8.5^m. From JD = 2 453 000 until the present, the brightness has experienced irregular fluctuations within 9.00^m–9.25^m. In contrast to Miras, it is difficult to compare the variations of the maser emission of the semi-regular variable R Crt with its optical activity.

Emission in the 1612 and 1667 MHz OH lines was first detected in 1977 [28]. Subsequent spectra of the OH lines were published in [29]. Polarization observations of the OH maser in R Crt were conducted on the Nanç Radio Telescope by Szymczak et al. [9–11] and Etoka et al. [12]. In particular, the variability of the R Crt maser over 13 years in 1982–1995 was studied in [11, 12]. While the general appearance of the total intensity profiles I at 1665 and 1667 MHz was preserved, variations in the degree of circular polarization were noted, which were attributed to turbulence in the circumstellar envelope and possible reversal of the sign of the global magnetic field of the star [11, 12]. In addition, the polarized OH 1665 and 1667 MHz emission of R Crt [14] was mapped with MERLIN in December 1995.

We observed the R Crt OH maser in the 1612 and 1667 MHz OH lines on November 21, 2007 and January 3, 2008 (Fig. 5). No emission in the 1612 MHz line was detected, with a 3σ upper limit of ∼0.2 Jy; i.e., the R Crt OH maser (like T Lep and R LMi) belongs to Class I.

Our measured 1667 MHz profiles are qualitatively consistent with those observed in [11, 12, 14, 28, 29]. The profiles have a similar structure in both of our observing sessions (Table 2): four emission features encompassing the stellar radial velocity of R Crt, $V^*_{\rm LSR} = +10.2$ km/s.

The most intense feature (which also has the greatest blueshift relative to $V^*_{\rm LSR}$) is at $V_{\rm LSR} = +2.74$ km/s. Its flux density is $F_{\rm max} = 2.7$ Jy in the first session and 1.9 Jy in the second. This feature is elliptically polarized (nonzero Stokes parameters Q, U, and V). In both cases, there is a Zeeman pattern in the V profile with features at $V_{\rm LSR} = +2.47$ and +2.88 km/s. This line splitting corresponds to the line-of-sight component of the magnetic field that is directed away from the observer and has a strength of 1.16 mG. This feature is also present in the MERLIN map [14], where it coincides with the optical position of the star. This feature is probably formed at the near side of the expanding circumstellar envelope; it represents a "radio image" of the star amplified by the maser. As is noted in the Introduction, in this case, the high degree of polarization of the feature (both circular and linear) is explained by the fact that, in contrast to the emission of weaker features at $V > V^*_{\rm LSR}$, its emission does not pass through the inner layers of the circumstellar envelope, where the electron density is higher, so that it does not undergo Faraday depolarization.

5. CONCLUSION

We carried out systematic observations of the polarization of the maser emission for a large sample of late-type stars on the upgraded radio telescope of the Nançay Radio Astronomy Observatory (France) from October 2007 to June 2009. Most of these stars (54 of 70) are long-period Mira variables, while the rest are semi-regular variables or are not classified as variable stars (the infrared sources IRC−20176 and IRC−10414). As a rule, Mira variables are Class I

OH masers, whose strongest emission is in the main lines at 1665 and 1667 MHz; this is true of the Miras considered here, T Lep and R LMi, as well as the semi-regular variable R Crt. We have detected class I OH maser emission in the Mira T Lep for the first time.

The fraction of stars of the sample with polarized OH emission is fairly high: 41 of the 53 objects for which emission was detected. Linear polarization was found for many stars, which is not so typical of OH masers; circular polarization is more frequently encountered. In a number of stars (including T Lep, R LMi, and R Crt), the profile of Stokes V (the difference between the RC and LC profiles) demonstrates a characteristic structure with a change of the sign of V within a narrow frequency interval. This structure can be interpreted as Zeeman splitting, and used to estimate the line-of-sight axial component of the magnetic field. For late-type stars, the maser line profiles usually consist of one or two emission features, which are not blended with each other. Therefore, it is easier to reveal the Zeeman pattern in the Stokes profiles in stellar masers than in masers associated with star-forming regions (even in single-dish observations), where the line profile is formed of a multitude of overlapping peaks with different polarization states. As a result, we have obtained the following line-of-sight magnetic field components: 0.46 mG in T Lep, 2.32 mG in R LMi, and 1.16 mG in R Crt.

Masing regions in late-type stars are at distances of $\sim 10^{15}-10^{16}$ cm from the center of the star. If the stellar magnetic field has a dipole character whose strength decreases inversely proportional to the cube of the distance, an extrapolation of the obtained fields to the stellar photosphere (i.e., to a distance of about an astronomical unit from the center) implies magnetic fields near the photosphere reaching thousands of Gauss. Multi-epoch polarimetric observations of these same stars aimed at detecting possible cyclicity in their magnetic activity are of interest. So far, OH spectra for time intervals of the order of the variability cycles have been obtained for only a few of the stars observed by us (T Lep, GX Mon, HU Pup, U Her, UU Peg; Table 2).

Observations with higher spectral resolution are also desirable, since the observed splitting of the OH lines is small (about two–three spectral channels, or less than 0.5 km/s), and more precise estimates of the magnetic fields require knowledge of the detailed structure of the Stokes profiles.

Detailed results of our polarization observations and an analysis of these observations for the entire sample of stars will be given in forthcoming publications.

ACKNOWLEDGMENTS

The authors are grateful to the staff of the Nançay Radio Astronomy Observatory for their help with the observations. This work was supported by the Russian Foundation for Basic Research (project nos. 06-02-16806 and 09-02-00963). The data of the American (AAVSO) and French (AFOEV) associations of variable star observers were used in this study.

REFERENCES

1. P. J. Benson, I. R. Little-Marenin, T. C. Woods, et al., Astrophys. J. Suppl. Ser. **74**, 911 (1990).
2. A. H. Cook, Mon. Not. R. Astron. Soc. **140**, 299 (1968).
3. I. S. Shklovsky, Astron. Zh. **46**, 3 (1969) [Sov. Astron. **13**, 1 (1969)].
4. R. D. Davies, in *Galactic Radio Astronomy*, Ed. by F. J. Kerr and S. C. Simonson (Reidel, Dordrecht, Boston, 1974), p. 275.
5. V. V. Burdyuzha and D. A. Varshalovich, Astron. Zh. **52**, 1178 (1975) [Sov. Astron. **19**, 705 (1975)].
6. M. J. Claussen and J. D. Fix, Astrophys. J. **263**, 153 (1982).
7. N. Ukita and A. M. Le Squeren, Astron. Astrophys. **138**, 343 (1984).
8. P. N. Kholopov, N. N. Samus', V. P. Goransky, et al., *General Catalog of Variable Stars*, vols. 1–3 (Nauka, Moscow, 1985–1987) [in Russian]; http://www.sai.msu.su/groups/cluster/gcvs/gcvs//iii/iii.dat.
9. M. Szymczak and A. M. Le Squeren, Mon. Not. R. Astron. Soc. **304**, 415 (1999).
10. M. Szymczak, A. M. Le Squeren, P. Sivagnanam, et al., Astron. Astrophys. **297**, 494 (1995).
11. M. Szymczak, L. Błaszkiewicz, S. Etoka, and A. M. Le Squeren, Astron. Astrophys. **379**, 884 (2001).
12. S. Etoka, L. Błaszkiewicz, M. Szymczak, and A. M. Le Squeren, Astron. Astrophys. **378**, 522 (2001).
13. M. Szymczak, R. J. Cohen, and A. M. S. Richards, Mon. Not. R. Astron. Soc. **297**, 1151 (1998).
14. M. Szymczak, R. J. Cohen, and A. M. S. Richards, Mon. Not. R. Astron. Soc. **304**, 877 (1999).
15. M. Szymczak and E. Gérard, Astron. Astrophys. **423**, 209 (2004).
16. M. Szymczak and E. Gérard, Astron. Astrophys. **494**, 117 (2009).
17. L. S. Celis, Astron. J. **89**, 1343 (1984).
18. P. Te Lintel Hekkert, J. L. Caswell, H. J. Habing, et al., Astron. Astrophys. Suppl. Ser. **90**, 327 (1991); ftp://cdsarc.u-strasbg.fr/pub/cats/J/A+AS/90/327.
19. B. M. Lewis, P. David, and A. M. Le Squeren, Astron. Astrophys. Suppl. Ser. **111**, 237 (1995).
20. J. R. D. Lépine, A. M. Le Squeren, and E. Scalise, Jr., Astrophys. J. **225**, 869 (1978).

21. P. F. Bowers and W. Hagen, Astrophys. J. **285**, 637 (1984).
22. S. Deguchi, J. Nakashima, and R. Balasubramanyam, Publ. Astron. Soc. Jpn. **53**, 305 (2001).
23. F. Herpin, A. Baudry, C. Thum, et al., Astron. Astrophys. **450**, 667 (2006).
24. M. Szymczak and A. M. Le Squeren, Mon. Not. R. Astron. Soc. **276**, 635 (1995).
25. W. J. Wilson and K. W. Riegel, Astron. Astrophys. **22**, 473 (1973).
26. R. Fillit, M. Gheudin, Nguyen-Quang-Rieu, et al., Astron. Astrophys. **21**, 317 (1972).
27. F. Colomer, M. J. Reid, K. M. Menten, and V. Bujarrabal, Astron. Astrophys. **355**, 979 (2000).
28. A. M. Le Squeren, A. Baudry, J. Brillet, and B. Darchy, Astron. Astrophys. **72**, 39 (1979).
29. D. F. Dickinson, B. E. Turner, P. R. Jewell, and P. J. Benson, Astron. J. **92**, 627 (1986).

Translated by G. Rudnitskii